Significant Visible Photoactivity and Antiphotocorrosion Performance of CdS Photocatalysts after Monolayer Polyaniline Hybridization

Hao Zhang and Yongfa Zhu*

Department of Chemistry, Tsinghua University, Beijing, 100084, People's Republic of China

Received: November 17, 2009; Revised Manuscript Received: March 02, 2010

The dramatic enhanced visible light photocatalytic activity and excellent antiphotocorrosion performance of CdS photocatalysts were obtained after hybridized by monolayer polyaniline. The as-prepared PANI-CdS hybrid photocatalysts reveal the outstanding photocatalytic activity and photoelectrical conversion efficiency which can improve about 2.5 and 1.8 times that of the pure CdS, respectively. Significantly, the issue of photocorrosion, a congenital disadvantage of CdS photocatalysts, has been solved completely after hybridization. The mechanisms on enhancement of photocatalytic activity and antiphotocorrosion performance have been emphasized. Under visible light irradiation, photogenerated electrons in LUMO of PANI injected into the conduction band of CdS, photogenerated holes in the valence band of CdS transferred to the photocatalysts surface through HOMO of PANI. The rapid transferring of hole and high separation efficiency of electron−hole pairs lead to the dramatically enhanced photoactivity and completely inhibited photocorrosion.

1. Introduction

Semiconducting photocatalysts have attracted extensive attention in recent years owing to their great potential in environmental purification and hydrogen energy production.[1−3] So far, TiO_2 is still the most investigated photocatalyst, but the wide energy gap (3.2 eV) has hindered its sufficient utilization of sunlight.[4] Compared to TiO_2, CdS with a direct bandgap of 2.42 eV is considered to be an excellent visible-light-responsive material for photocatalysis and solar cells.[5,6] Unfortunately, critical drawbacks of CdS remain: the photogenerated electron−hole pair's separation efficiency is very low, and moreover, it is easy to photocorrode in aqueous media containing oxygen when exposed to visible light,[7,8] which are not favorable for its applications in environmental mediation and solar conversion. Enormous efforts have been devoted to increase photoactivity and suppress photocorrosion, such as combining CdS with another semiconductor,[9,10] or embedding CdS particles in mesoporous materials[11,12] or polymer matrix to form hybrid photocatalysts,[13,14] or exploiting alternative preparation approaches.[15,16] However, few of the above-mentioned attempts have proven to be successful in increasing both the photoactivity and antiphotocorrosion.

Recently, we have exploited a novel process on semiconducting photocatalysts by hybridizing with delocalized conjugated materials such as fullerene C60,[17,18] graphite,[19] or conducting polyaniline (PANI).[20,21] In these researches, the delocalized conjugated materials are matched well with the photocatalysts in energy level and an intensive interface hybrid effect emerged between these two materials, arousing rapid charge separation and slow charge recombination in the electron-transfer process. It was well-known that PANI is an efficient conductive polymer with unique electron and hole transporting properties.[22] In a previous paper, we have demonstrated that the hybridization by monolayer PANI can enhance the photocatalytic activity and inhibit the photocorrosion of ZnO remarkably.[21] CdS and PANI are also well-matched in energy level.[23] The present work explores further this topic considering the case of CdS, a visible-light-driven photocatalysts. It is expected that the surface hybridization by PANI can make CdS not only obtain higher efficiency but also avoid photocorrosion.

Herein, PANI monolayer-hybrid CdS photocatalysts were fabricated by the chemisorption method. It was demonstrated that a hybrid effect existed between CdS and PANI that caused the high separation efficiency of photogenerated electron−hole pairs. This hybrid effect results in the photocorrosion of CdS being completely suppressed and produced enhanced photoactivity. Our efforts propose a new scheme to design novel cadmium-chalcogen-based photocatalysts to bear tremendous hope in helping solve the serious environmental and energy challenges nowadays.

2. Experimental Section

2.1. Materials Preparation. PANI (molecular weight $\sim 10^5$) was purchased from Jilin Zhengji Corp, PR China. CdS nanocrystals were prepared by a solvothermal process.[24] All chemicals were of analytical grade and were used without further purification. The PANI-CdS photocatalysts were fabricated as follows: an amount of CdS powder was added to 100 mL of 0.45 g L^{-1} PANI (THF) solution with sonication for 30 min, then the mixture was stirred for 24 h. The suspension was filtrated and the precipitate was washed with deionized water three times, then transferred to an oven to dry at 60 °C for 24 h; herein, a series of PANI-CdS photocatalysts from 1.0 to 10.0 wt % were synthesized. To test the photoelectrochemical performance of PANI-CdS, the photocatalysts dispersed in ethanol solution were evenly spread onto ITO (Indium Tin Oxide) glass substrates (3 cm × 2 cm) with a sheet resistance of 15 Ω. After being dried, the as-prepared electrodes were dried at 80 °C for 24 h.

2.2. Characterization. XRD patterns were recorded on a Bruker D8 Advance XRD diffractometer with Cu Kα radiation. Diffusion reflection spectra (DRS) were carried out on a Hitachi U-3010 instrument with $BaSO_4$ as the reference sample. Porosity was monitored with a Demo 2020 V3.00 G instrument from the nitrogen adsorption−desorption isotherms obtained at 77

* To whom correspondence should be addressed. Phone: +86-10-62783586. Fax: +86-10-62787601. E-mail: zhuyf@tsinghua.edu.cn.

10.1021/jp910930t
Published on Web 03/11/2010

K. The Brunauer−Emmett−Teller (BET) surface area measurements were performed by a Micromeritics (ASAP2010 V5.02H) surface area analyzer. TG-DTA analyses were taken over a STA409 thermal analyzer in N_2 atmosphere between room temperature and 900 °C at a heating rate of 10 deg min^{-1}. FTIR spectra were measured by using a Perkin-Elmer System 2000 infrared spectrometer with KBr as the reference sample. Raman spectra were recorded on a RM 2000 microscopic confocal Raman spectrometer (Renishaw Company) with an excitation of 633 nm laser light. TEM and HRTEM images were obtained by JEM2010 transmission electron microscope operated at the accelerating voltage of 120 and 200 kV, respectively. Total organic carbon (TOC) was measured with a Tekmar Dohrmann Apollo 9000 TOC analyzer. Photoelectrochemical experiments were measured on an electrochemical system (CHI-660B, China).

2.3. Photocatalytic Experiments. The photocatalytic activity was evaluated by the degradation of Methylene Blue (MB) under visible light irradiation ($\lambda > 450$ nm). The visible light was obtained by a 500 W xenon lamp (Institute of Electric Light Source, Beijing) with a 450 nm cutoff filter to ensure the desired irradiation light. The average light intensity was 33.2 $mW \cdot cm^{-2}$ measured by a power meter from the Institute of Electric Light Source, Beijing. A suspension containing a powdered catalyst (100 mg) and a fresh aqueous solution of MB (200 mL, 20 mg L^{-1}) was ultrasonicated for 10 min and magnetically stirred in the dark for about 30 min to establish an adsorption/desorption equilibrium of the MB species. The suspensions were kept under constant air-equilibrated conditions before and during illumination. At certain time intervals, 2 mL aliquots were sampled and centrifuged to remove the particles. The filtrates were analyzed by recording variations of the maximum absorption band (633 nm), using a Hitachi U-3010 UV−vis spectrophotometer. The active oxidants generated in the photocatalytic process could be measured through trapping by *tert*-butyl alcohol (*t*BuOH) and disodium ethylenediamine tetraacetate (EDTA-2Na).

2.4. Photoelectrochemical Measurements. Photoelectrochemical tests were carried out in a conventional three-electrode, single-compartment quartz cell, filled with 0.1 M Na_2SO_4 electrolyte (130 mL), using a potentiostat. The ITO/CdS or ITO/PANI-CdS electrodes served as the working electrode. The counter and the reference electrodes were platinum black plate and saturated calomel electrode (SCE), respectively. A 500 W xenon lamp was used as the excitation light source for visible irradiation. Electrochemical impedance spectra (EIS) were recorded in the potentiostatic mode. The amplitude of the sinusoidal wave was 10 mV, and the frequency range of the sinusoidal was from 100 kHz to 0.05 Hz. For maximum incident photon-to-electron conversion efficiency (IPCE) measurements, the solution of 0.05 M I_2 and 0.5 M LiI in propylene carbonate was used as electrolyte. The monochromatic light was from a 500 W xenon lamp, which was passed through a SAP301 grating monochromator (Zolix Instruments Co., Ltd., Beijing), and the wavelength was selected at 10 nm intervals between 400 and 690 nm.

3. Results and Discussion

3.1. Enhancement of Photocatalytic Activity. The photodegradation of MB under visible light irradiation ($\lambda > 450$ nm) was carried out to investigate the performance of photocatalysts. The pure CdS and the mechanic blend of CdS and PANI (5.0 w/w %) were used as the reference photocatalysts. Seen from Figure 1, various PANI-CdS samples had enhanced visible light activity compared with the reference photocatalysts. The PANI-CdS (5.0%) photocatalysts exhibited the highest activity that could degrade 20 ppm MB by 92% within 5 h. While, the reference photocatalysts had poor photocatalytic activity that could degrade only about 60% MB within 5 h. The total organic carbon (TOC) removal was also investigated during the photocatalysis reaction. After the photocatalytic process over PANI-CdS for 5 h, the TOC concentration decreased from 20.85 ppm to 2.11 ppm, namely 90% of TOC was removed by photocatalytic oxidation. The photodegradation process followed pseudo-first-order kinetics and the maximum rate constant k (for PANI-CdS (5.0%), 0.491 h^{-1}), was about 2.5 times that of pure CdS (0.197 h^{-1}). It also could be seen from Figure 1B that the loading amount of PANI had a great influence on the activity of the as-prepared photocatalysts. With the PANI content increasing, the photocatalytic performance of PANI-CdS did not enhance monotonously. When the PANI content was relatively low (<5.0%), the photocatalytic activity increased continuously; when the PANI content was relatively high (>5.0%), the photocatalytic activity decreased with increasing PANI content. The optimal PANI content was approximately 5.0%. At higher PANI content (>5.0%), PANI accumulated on the CdS surface might cause a reduced adsorption of MB and promote recombination of photogenerated carriers, resulting in a decrease of photocatalytic efficiency. Noticeably, mechanical blend did not increase the photocatalytic activity, which implies there is no interaction between CdS and PANI in the mechanical mixture. That the hybridization had enhanced the photocatalytic activity of the CdS semiconductor implies there may be some interaction between CdS and PANI.

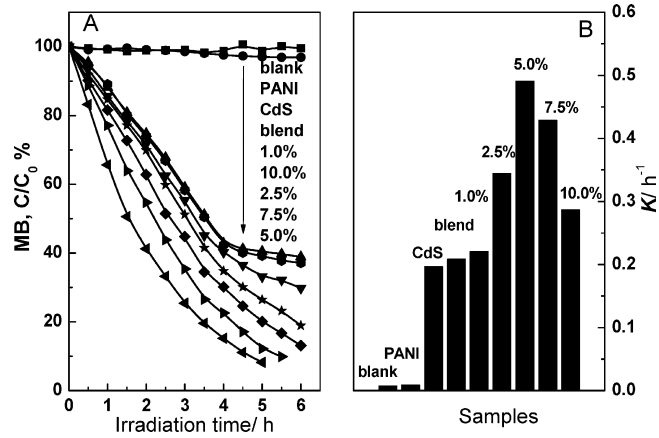

Figure 1. Photocatalytic degradation of MB over the as-prepared samples under visible light irradiation ($\lambda > 450$ nm): (A) the photodegradation plots and (B) rate constant k as a function of PANI content, catalyst loading, 0.5 g L^{-1}; MB, 2×10^{-5} M.

3.2. Inhibition of Photocorrosion. XRD patterns and TEM images were used to evaluate the photostability of the catalyst before and after photodegradation of MB for four recycles. In Figure 2, it is revealed that PANI-CdS (5.0%) had a crystalline phase structure similar to that of CdS and no peaks assigned to PANI were observed because the PANI layer was too thin. For pure CdS, after photocatalytic recycles, the crystalline phase structure was destroyed disastrously, indicating a severe photocorrosion had taken placed. Whereas XRD patterns of PANI-CdS (5.0%) had no notable differences before and after the photocatalytic recycles, indicating that PANI-CdS is photostable and not photocorroded, in TEM images, both CdS and PANI-CdS (5.0%) photocatalysts consisted of agglomerated approximately spherical particles with diameters of 10−20 nm (see the Supporting Information, Figure S1). For PANI-CdS (5.0%), it revealed no great loss in morphology before and after photocatalytic recycles, further confirming that PANI-hybrid

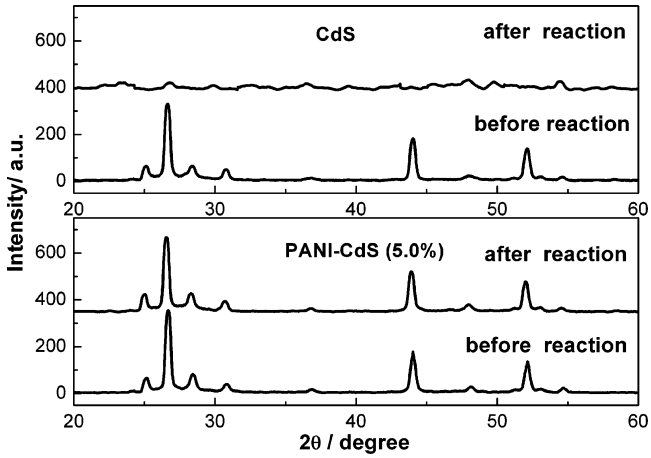

Figure 2. XRD patterns of CdS and PANI-CdS (5.0%) photocatalysts before and after photodegradation of MB under visible light irradiation ($\lambda > 450$ nm) for four recycles.

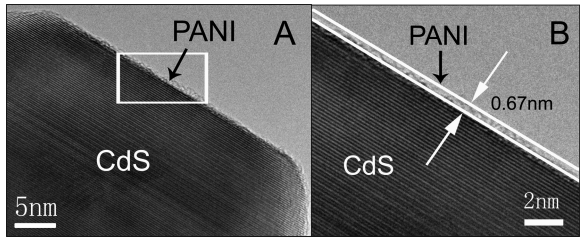

Figure 3. (A) HRTEM images of PANI-CdS (5.0%) and (B) its partial magnified image.

CdS did not photocorrode. As for pure CdS, after photocatalytic recycles, the spherical particles disappeared, and only flocculent morphologies existed, indicating that the crystalline structure of the CdS had already been demolished. The TEM result was in agreement with the results of XRD tests, further indicating that the PANI hybrid layer could protect the CdS semiconductor from photocorrosion completely.

3.3. Hybrid Structures. XRD patterns of PANI-CdS photocatalysts exhibited similar diffraction peaks as those for CdS (see the Supporting Information, Figure S2). DRS (see the Supporting Information, Figure S3) illustrated that compared with the pure CdS, PANI-hybridized CdS showed almost the same absorbance edge but extended the absorbance to the visible region as far as 800 nm. Further, as for CdS and PANI-CdS (5.0%), there were no appreciable changes in TEM images, nitrogen adsorption isotherms, and BJH pore size distributions (see the Supporting Information, Figure S4), and BET surface area (118.2 ± 2 and 114.3 ± 2 $m^2 \cdot g^{-1}$, respectively) before and after hybridization. Because the phase structure and surface properties of CdS remained changeless, we may conclude that the separation of the photogenerated electrons and holes plays an important part in the enhancement of the photocatalytic activity of the hybrid photocatalysts.

The high separation and transferring efficiency of charge carriers is mainly related to the interface property of PANI-CdS photocatalysts. HRTEM images of PANI-CdS (5.0%) were shown in Figure 3. The images revealed that the CdS particles were surrounded by a small amount of PANI, and the thickness of the PANI shell is about 1 nm. In Figure 3B, a partial magnified HRTEM image of PANI-CdS (5.0%) revealed that the lattice structure of CdS was very orderly and the outer noncrystal PANI layer was distinctly different from the CdS core. The PANI layer with catenulate structure adsorbed evenly and stably on the CdS surface with a thickness of about 0.67 nm, which was close to the scale of monolayer PANI;[20,21] so, it can be supposed the PANI molecule was dispersed on the surface of CdS with a monolayer structure.[18,20] The TG curves of PANI-CdS (5.0%) (see the Supporting Information, Figure S5) underwent a two-step weight loss pattern, the initial one occurring from 50 to 200 °C attributed to desorption of solvent and the second about 4.72% from 200 to 650 °C was attributed to the decomposition of PANI.[25] This was nearly consistent with the amount of monolayer PANI dispersed on CdS, 5.0%. In the DTA curve of PANI-CdS (5.0%) (see the Supporting Information, Figure S5), the endothermic peak at 300 °C was due to the chemical desorption and decomposition of PANI, which was higher than that of pure PANI,[23,26] and the phase transformation endothermic peak of pure CdS at 660 °C[25] shifted to 710 °C, indicating a strong chemical interaction took place and PANI formed a chemical adsorption on the CdS surface. According to all the above results, it could be concluded that the PANI molecule was bonded on the surface of CdS and formed a monolayer structure.

Raman and FTIR spectra were studied to obtain the information on the interface interaction of CdS and PANI (see the Supporting Information, Figure S6). In Raman spectra of the PANI-CdS photocatalyst samples, the main characteristic bands of PANI all appeared. However, compared to pure PANI, the bands at 1605 (benzenoid unit vibration mode), 1476 (quinonoid unit vibration mode), and 1173 cm^{-1} (C−H bend mode)[27] all moved to lower wavenumber. The red shift of these bands suggested that the bond strengths of C═N (C═C) and C−N were weakened. Moreover, in FTIR spectra, the peaks of pure PANI at 1560 (C═N and C═C stretching mode) and 1294 cm^{-1}(C−N stretching mode),[27,28] shifted to lower wavenumber, also indicating that all these chemical bonds were weakened. According to the results of Raman and FTIR, the hybridization between CdS and PANI resulted in an intense interface interaction and the chemical-adsorbed monolayer PANI structure caused a hybrid effect between PANI and CdS. This hybrid effect was essential to promoting the separation efficiency of photogenerated carriers and enhancing photocatalytic activity and antiphotocorrosion performance.

3.4. Enhancement of Photoelectrochemical Activity. All kinds of photoelectrochemical tests, such as photocurrent spectra, EIS, and IPCE, can be used to investigate the photoelectrochemical activity. The photocurrent was enhanced after hybridization by PANI, and with the PANI content increasing, the photocurrent of the ITO/PANI-CdS electrode was first enhanced then declined though it was much larger than that of the ITO/CdS electrode and the ITO/PANI-CdS (blend) electrode (see the Supporting Information, Figure S7). The ITO/PANI-CdS (5.0%) electrode had the largest photocurrent, which was 2.4 and 2.1 times that of the ITO/CdS and ITO/PANI-CdS (blend) electrodes, respectively. The enhanced photocurrent generation was also observed in the reports of oligoaniline/CdS films.[29−31] EIS was used to investigate the photogenerated charge separations process and the radius of the arc on the EIS Nynquist plot reflected the reaction rate occurring at the surface of the electrode.[32] The arc radius on EIS Nynquist plots of all ITO/PANI-CdS electrodes was smaller than that of the ITO/CdS and ITO/PANI-CdS (blend) electrodes (see the Supporting Information, Figure S8), which meant a more effective charge separation and faster interfacial charge transferring had occurred after hybridization. The smallest arc radius representated the highest photogenerated charge separations efficiency, which was obtained on the ITO/PANI-CdS (5.0%) electrode. In Figure 4, the incident photocurrent conversion spectra of all the electrodes

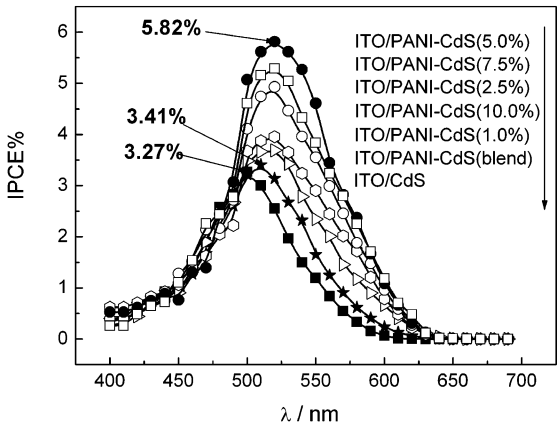

Figure 4. The incident photocurrent coversion spectra of ITO/CdS and various ITO/PANI-CdS film electrodes.

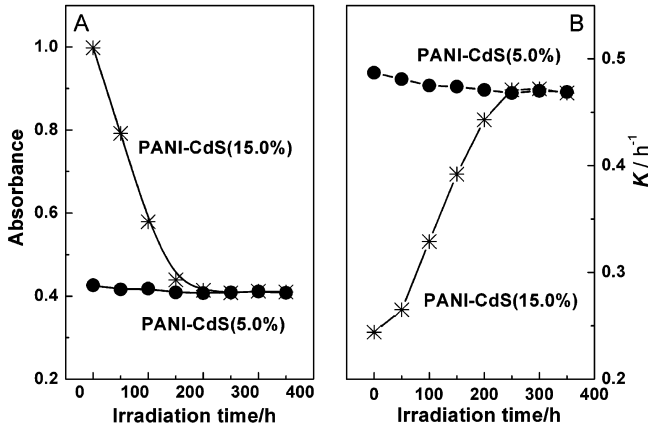

Figure 5. The influence of simulated solar light preillumination upon the dispersed amount of PANI on CdS surface (light density: 1.8 mW·cm^{-2}): (A) the changes of absorbance at typical wavelength (λ = 650 nm) and (B) the plots of visible degradation rates of MB.

exhibited similar photoresponse in the visible region and all of the ITO/PANI-CdS electrodes showed notablely improved IPCE values[33] compared to the ITO/CdS and ITO/PANI-CdS (blend) electrodes. The maximum IPCE value of 5.82% was observed over the ITO/PANI-CdS (5.0%) electrode, which was 1.78 and 1.70 times larger than that of the ITO/CdS (3.27%) and ITO/PANI-CdS (blend) electrodes (3.41%), respectively. The enhancement of photoelectrochemical activity is due to a higher charge separation and transferring efficiency, which proved further that the hybridization of CdS and PANI was an effective way to improve photocatalytic efficiency.

3.5. Photostability of the PANI Layer. The hybrid effect could enhance the photostability of the PANI layer. From TG-DTA curves, it is revealed that the stability of PANI was increased after hybridization. It was also confirmed that the monolayer PANI (in PANI-CdS (5.0%)) had excellent photostability because there were no distinct changes in DRS and photocatalytic activity even after 350 h of simulated solar irradiation, whereas, the multilayer PANI (in PANI-CdS (15.0%)) had poor photostability and was photodegraded continuously (see the Supporting Information, Figure S9). Figure 5 is a representive graph of the changes of absorbance at typical wavelength (λ = 650 nm) and the visible degradation rates of MB. It is worth mentioning that after irradiated for as long as 350 h, the absorbance and the photocatalytic activity of these two photocatalysts reached the same values which were approximately equal to those of the original PANI-CdS (5.0%). The reason for the above results was that the monolayer PANI

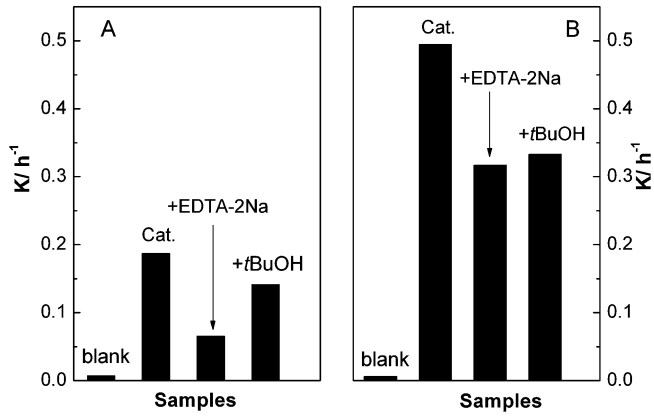

Figure 6. The plots of photogenerated carriers trapping in the system of photodegradation of MB over (A) CdS and (B) PANI-CdS (5.0%), respectively (EDTA-2Na and *t*BuOH: 10^{-3} M).

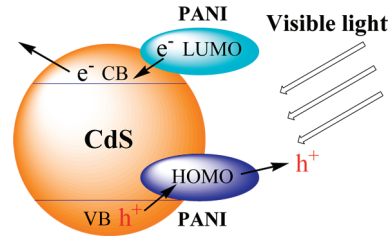

Figure 7. The mechanism scheme of the visible light photocatalysis process over PANI-CdS photocatalysts.

(chemical-adsorption) could be maintain undecomposed due to hybrid effect, while, the multilayer PANI (physical-adsorption) had no hybrid effect and was continuously photodegraded until only monolayer PANI remained. So the strong hybrid effect could only emerge on the interface in the monomolecular layer scale.

3.6. Mechanism of Visible Photoactivity and Photocorrosion Inhibition. It is of importance to detect the main oxidant in the photocatalytic process for investigating the photocatalytic mechanism. Detecting the main oxidant could be carried out through the radicals and holes trapping experiments.[34] As shown in Figure 6A, in the system containing CdS photocatalysts, under visible light irradiation CdS was induced to generate electron−hole pairs, yielding radical and hole oxidants. This revealed that the photodegradation activity of MB was suppressed when either *t*BuOH (radical scavenger) or EDTA-2Na (hole scavenger) was added. Moreover, the photocatalytic process was decelerated distinctively after EDTA-2Na was added. This indicated that photogenerated holes were the main oxidant and the photocorrosion caused by holes was the dominant photocorrosion in this system.[35] As for the system of PANI-CdS (5.0%) and MB (see Figure 6B), the photodegradation of MB was suppressed after the injection of *t*BuOH or EDTA-2Na. This indicated that both holes and radicals were the main oxidants in this system.[36]

On the basis of the results of photocatalytic and photogenerated carrier trapping tests, the enhancement of visible photoactivity was mainly due to the high efficiency of charge separation induced by the hybrid effect of PANI and CdS. A schematic mechanism of the charge separation and photocatalytic process over the PANI-CdS photocatalyst is shown in Figure 7. It was reported that CdS and PANI are matched well in energy level:[23] the conduction band (CB) position of CdS was lower than the LUMO of PANI, so the former could act as a sink for the photogenerated electrons in the hybrid photocatalysts; the valence band (VB) position of CdS was lower

than the HOMO of PANI, so the later could act as an acceptor for the photogenerated holes in the hybrid photocatalysts. Both CdS and PANI can be excited by visible light to produce photogenerated carriers and excited electrons, respectively. The excited state electrons in PANI can readily inject into CB of CdS. Simultaneously, the photogenerated holes in VB of CdS are able to move freely to the composites surface through HOMO of PANI. So herein, photogenerated electrons and holes moved in opposite directions, reducing the recombination probability and making charge separation more efficient which lead to a higher photocatalytic activity. Concurrently, photogenerated holes rapidly transferring to the solution successfully promoted the inhibition of photocorrosion.

4. Conclusions

In summary, besides enhanced visible photocatalytic activity, a further cardinal advantage of PANI-CdS hybrid photocatalysts is excellent photoelectric conversion efficiency and antiphotocorrosion property, all of which are attributed to the interface hybrid effect between PANI and CdS. It may be of catholicity that the modulation by means of chemisorptions can help semiconductors such as cadmium-chalcogen-based photocatalysts to suppress the photocorrosion and enhance the photoactivity. The present hybrid visible-light-driven photocatalyst is a promising photocatalytic and photoelectric conversion material of good potential applications for environmental purification and hydrogen production by using solar energy.

Acknowledgment. This work was partly supported by the National Natural Science Foundation of China (20925725 and 20673065) and National Basic Research Program of China (2007CB613303).

Supporting Information Available: TEM images, XRD patterns, diffuse reflectance spectra, N_2 adsorption−desorption isotherms, BJH pore size distribution plots, TG-DTA curves, FT-IR and Raman spectra, photocurrent graphs, EIS Nynquist plots, the stability experiment of photocatalysts. This material is available free of charge via the Internet at http://pubs.acs.org.

References and Notes

(1) Hoffmann, M. R.; Martin, S. T.; Choi, W. Y.; Bahnemann, D. W. *Chem. Rev.* **1995**, *95*, 69–96.
(2) Fujishima, A.; Zhang, X. T.; Tryk, A. D. *Int. J. Hydrogen Energy* **2007**, *32*, 2664–2672.
(3) Kudo, A. *Int. J. Hydrogen Energy* **2007**, *32*, 2673–2678.
(4) Chen, X.; Mao, S. S. *Chem. Rev.* **2007**, *107*, 2891–2959.
(5) Rauh, D. R. In *Semiconductor Electrodes*; Finklea, H. O., Ed.; Elsevier: Amsterdam, The Netherlands, 1988; Chapter 6.
(6) Matsumura, M.; Saho, Y.; Tsubomura, H. *J. Phys. Chem.* **1983**, *87*, 3807–3808.
(7) Becquerel, W. R. Photovoltaic effect in binary compounds. *J. Chem. Phys.* **1960**, *32*, 1505–1514.
(8) Gerischer, H. *Pure Appl. Chem.* **1980**, *52*, 2649–2667.
(9) Yamada, S.; Nosaka, A. Y.; Nosaka, Y. *J. Electroanal. Chem.* **2005**, *585*, 105–112.
(10) Jang, J. K.; Ji, S. M.; Bae, S. W.; Son, H. C.; Lee, J. S. *J. Photochem. Photobiol. A* **2007**, *188*, 112–119.
(11) Guan, G. Q.; Kida, T.; Kusakabe, K.; Kimura, K.; Fang, X. M.; Ma, T. L.; Abe, E.; Yoshida, A. *Chem. Phys. Lett.* **2004**, *385*, 319–322.
(12) Ryu, S. Y.; Balcerski, W.; Lee, T. K.; Hoffmann, M. R. *J. Phys. Chem. C* **2007**, *111*, 18195–18203.
(13) Khanna, P. K.; Gokhale, R. R.; Subbarao, V. V. V. S.; Singh, N.; Jun, K.-W.; Das, B. K. *Mater. Chem. Phys.* **2005**, *94*, 454–459.
(14) Jang, J.; Kim, S. H.; Lee, K. J. *Chem. Commun.* **2007**, 2689–2691.
(15) Jing, D.; Guo, L. *J. Phys. Chem. B* **2006**, *110*, 11139–11145.
(16) Bao, N.; Shen, L.; Takata, T.; Domen, K. *Chem. Mater.* **2008**, *20*, 110–117.
(17) Zhu, S. B.; Xu, T. G.; Fu, H. B.; Zhao, J. C.; Zhu, Y. F. *Environ. Sci. Technol.* **2007**, *41*, 6234–6239.
(18) Fu, H. B.; Xu, T. G.; Zhu, S. B.; Zhu, Y. F. *Environ. Sci. Technol.* **2008**, *42*, 8064–8069.
(19) Zhang, L. W.; Fu, H.; Zhu, Y. F. *Adv. Funct. Mater.* **2008**, *18*, 2180–2189.
(20) Zhang, H.; Zong, R. L.; Zhao, J. C.; Zhu, Y. F. *Environ. Sci. Technol.* **2008**, *42*, 3803–3807.
(21) Zhang, H.; Zong, R. L.; Zhu, Y. F. *J. Phys. Chem. C* **2009**, *113*, 4605–4611.
(22) Kang, E. T.; Neoh, K. G.; Tan, K. L. *Prog. Polym. Sci.* **1998**, *23*, 277–324.
(23) Khanna, P. K.; Kulkarni, M. V.; Narendra, S.; Lonkar, S. P.; Subbarao, V. V. V. S.; Viswanath, A. K. *Mater. Chem. Phys.* **2006**, *95*, 24–28.
(24) Li, Y. D.; Liao, H. W.; Ding, Y.; Fan, Y.; Zhang, Y.; Qian, Y. T. *Inorg. Chem.* **1999**, *38*, 1382–1387.
(25) Khiew, P. S.; Huang, N. M.; Radiman, S.; Ahmad, M. S. *Mater. Lett.* **2004**, *58*, 516–521.
(26) Lu, X. F.; Yu, Y. H.; Chen, L.; Mao, H. P.; Zhang, W. J.; Wei, Y. *Chem. Commun.* **2004**, *4*, 1522–1523.
(27) Li, X. W.; Wang, G. C.; Li, X. X.; Lu, D. M. *Appl. Surf. Sci.* **2004**, *229*, 395–401.
(28) Xi, Y. Y.; Zhou, J. Z.; Guo, H. C.; Cai, C. D.; Lin, Z. H. *Chem. Phys. Lett.* **2005**, *412*, 60–64.
(29) Granot, E.; Patolsky, F.; Willner, I. *J. Phys. Chem. B* **2004**, *108*, 5875–5881.
(30) Yildiz, H. B.; Tel-Vered, R.; Willner, I. *Adv. Funct. Mater.* **2008**, *18*, 3497–3505.
(31) Tel-Vered, R.; Yildiz, H. B.; Willner, I. *Adv. Mater.* **2009**, *21*, 716–720.
(32) Leng, W. H.; Zhang, Z.; Zhang, J. Q.; Cao, C. N. *J. Phys. Chem. B* **2005**, *109*, 15008–15023.
(33) Hasobe, T.; Imahori, H.; Fukuzumi, S.; Kamat, P. V. *J. Phys. Chem. B* **2003**, *107*, 12105–12112.
(34) Xu, T.; Cai, Y.; O'Shea, K. E. *Environ. Sci. Technol.* **2007**, *41*, 5471–5477.
(35) Kamat, P. V.; Dimitrijevic, N. M.; Fessenden., R. W. *J. Phys. Chem.* **1987**, *91*, 396–401.
(36) Palominos, R.; Freer, J.; Mondaca, M. A.; Mansilla, H. D. *J. Photochem. Photobiol. A* **2008**, *193*, 139–145.

JP910930T